Lawrence Berkeley National Laboratory
Recent Work

Title
HYDROMAGNETIC WAVE PROPAGATION NEAR ION CYCLOTRON RESONANCE

Permalink
https://escholarship.org/uc/item/02s416nm

Authors
Boley, Forrest I.
Wilcox, John M.
DeSilva, Alan W.
et al.

Publication Date
1962-10-12

eScholarship.org Powered by the California Digital Library
University of California

UCRL-10381

University of California

Ernest O. Lawrence Radiation Laboratory

TWO-WEEK LOAN COPY

This is a Library Circulating Copy which may be borrowed for two weeks.. For a personal retention copy, call Tech. Info. Division, Ext. 5545

Berkeley, California

DISCLAIMER

This document was prepared as an account of work sponsored by the United States Government. While this document is believed to contain correct information, neither the United States Government nor any agency thereof, nor the Regents of the University of California, nor any of their employees, makes any warranty, express or implied, or assumes any legal responsibility for the accuracy, completeness, or usefulness of any information, apparatus, product, or process disclosed, or represents that its use would not infringe privately owned rights. Reference herein to any specific commercial product, process, or service by its trade name, trademark, manufacturer, or otherwise, does not necessarily constitute or imply its endorsement, recommendation, or favoring by the United States Government or any agency thereof, or the Regents of the University of California. The views and opinions of authors expressed herein do not necessarily state or reflect those of the United States Government or any agency thereof or the Regents of the University of California.

UCRL-10381

Sub. for pub. in Phys. Fluids

UNIVERSITY OF CALIFORNIA

Lawrence Radiation Laboratory
Berkeley, California

Contract No. W-7405-eng-48

HYDROMAGNETIC WAVE PROPAGATION NEAR ION CYCLOTRON RESONANCE

Forrest I. Boley, John M. Wilcox, Alan W. DeSilva, Peter R. Forman, Gordon W. Hamilton, and C. N. Watson-Munro

October 12, 1962

HYDROMAGNETIC WAVE PROPAGATION NEAR ION CYCLOTRON RESONANCE

Forrest I. Boley, John M. Wilcox, Alan W. DeSilva, Peter R. Forman, Gordon W. Hamilton, and C. N. Watson-Munro

Lawrence Radiation Laboratory
University of California
Berkeley, California

October 12, 1962

ABSTRACT

A torsional hydromagnetic wave is induced by application of an oscillatory radial electric field to one end of a cylindrical deuterium plasma located in a magnetic mirror field. The wave propagates in the axial direction to the center of the device, where a resonance occurs between the hydromagnetic wave frequency and the local ion cyclotron frequency. Wave magnetic-field measurements indicate that transfer of power from the 1-MW, 8.3-Mc oscillator to the hydromagnetic wave is about 65% efficient, and that more than 90% of the wave energy is transferred out of the wave at the resonance region.

HYDROMAGNETIC WAVE PROPAGATION NEAR ION CYCLOTRON RESONANCE*

Forrest I. Boley, John M. Wilcox, Alan W. DeSilva, Peter R. Forman, Gordon W. Hamilton and C. N. Watson-Munro†

Lawrence Radiation Laboratory
University of California
Berkeley, California

October 12, 1962

INTRODUCTION

Previous hydromagnetic wave experiments in highly ionized gaseous plasmas have largely confirmed the principal theoretical predictions regarding torsional Alfvén-wave propagation along a magnetic field when the wave frequency is well below the ion cyclotron frequency.[1-4] Additionally, two types of experiments concerned with wave frequencies near the ion cyclotron frequency have been reported. In one type, waves of transient character propagated in a variable, uniform magnetic field yield wave velocity and attenuation measurements.[5] In the other type, wave fields of longer time duration and substantial power level are induced in a magnetic minor geometry such that resonance with the local ion cyclotron frequency occurs at the minor minimum.[6,7]

The purpose of the experiments reported here is to extend the previous investigations of torsional Alfvén-wave propagation into that frequency domain where ion cyclotron resonance effects are important. This is done in a magnetic mirror field to provide some containment of the plasma. The experiments described here differ in two respects from other oscillator-driven ion cyclotron

---

† The Wills Plasma Physics Department, School of Physics, University of Sydney, Australia.

wave studies reported previously. First, torsional waves are generated by direct application to the plasma of an electric field between coaxial electrodes. Second, the magnetic field gradient along which wave propagation occurs is substantially larger than that used previously.

Of the three hydromagnetic wave modes that may propagate in a cylindrical plasma in an axial magnetic field, the torsional or Alfvén mode has a singularity when the wave frequency is equal to the ion cyclotron frequency. For this mode the mass motion is principally in the θ direction, at least for frequencies removed from the resonance frequency. For such low frequencies, the wave magnetic field is in the θ direction, and the wave electric field is radial. When the wave frequency approaches the ion cyclotron frequency, the electric field acquires a θ component and becomes in the local coordinate system elliptically polarized, with a direction of rotation in the same sense as the cyclotron motion. When the wave frequency becomes equal to the ion cyclotron frequency, the local electric field is circularly polarized, and in the absence of loss mechanisms the ions gain energy without limit. Appendix I gives details concerning the ion orbits under various conditions of magnetic field and of wave frequency. The presence of any loss mechanism--such as electron-ion collisions or phase mixing[8]--causes the wave energy to be rapidly transferred into thermal energy of ions or electrons, depending upon the process.

This paper is concerned with a torsional hydromagnetic mode that is induced in a cylindrical plasma under the condition that $\omega \approx \omega_{ci}/2$. The wave propagates into a region of decreasing magnetic field (hence decreasing ω_{ci}) until it reaches a region where $\omega = \omega_{ci}$ and the wave energy is lost.

The remainder of this paper is devoted to (a) a theoretical discussion of hydromagnetic wave propagation under the experimental conditions used,

(b) a description of the experimental apparatus used in making the wave measurements, (c) the wave measurements and their interpretation, and (d) comparison of the wave power with the input power supplied by the radio-frequency oscillator and with the power removed from the wave at ion cyclotron resonance.

THEORETICAL DISCUSSION

The exact theoretical treatment of hydromagnetic waves in spatially varying magnetic fields involves formidable mathematical difficulties. It is relatively easy, however, to solve the problem of waves in uniform fields. These results may be used with caution to gain information about the behavior of waves in nonuniform fields.

The problem of hydromagnetic waves in uniform fields has been considered by a number of authors.[3,9,10,11] We present here a summary of the assumptions and principal conclusions of the work by DeSilva, which includes the effects of the Hall currents and of electron-ion collisions.

The second moments of the Boltzmann equations for ions and electrons are the starting point.[12] A perturbation approach is used in which the fields associated with the wave are assumed small. Effects due to electron inertia, particle pressure, and viscosity are ignored, and charge neutrality is assumed. It is assumed that the solutions of interest will be of the form $f(r)e^{i(pz-\omega t)}$, where p may be complex--its imaginary part being the attenuation constant. The moment equations give an equation of motion

$$-i\omega p\ \underline{v}_i = \underline{j} \times \underline{B} \qquad (1)$$

and Ohm's law

$$\underline{E} + \underline{v}_i \times \underline{B} = \underline{\eta} \cdot \underline{j} + (1/en)(\underline{j} \times \underline{B}), \qquad (2)$$

which together with Maxwell's equations,

$$\nabla \times \underline{b} = \mu_0 \underline{j} \tag{3}$$

and

$$\nabla \times \underline{E} = i\omega \underline{b}, \tag{4}$$

constitute the set to be solved.

Here $\underline{B}$ is the static axial magnetic field, $\underline{\eta}$ is the resistivity tensor, n is ion-particle density, and the perturbation fields associated with the wave are $\underline{E}$, electric field; $\underline{b}$, magnetic field; $\underline{v}_i$, average ion velocity; and $\underline{j}$, the current density. The symbol ρ takes into account the effects of ion-neutral collisions and is defined by

$$\rho = \rho_0(1 + i\xi), \tag{5}$$

$$\rho_0 = \rho_i + \rho_n \frac{1}{1+\gamma^2}, \tag{6}$$

$$\xi = \frac{\rho_n}{\rho_0} \frac{\gamma}{1+\gamma^2}, \tag{7}$$

and

$$\gamma = \frac{\omega}{\nu_{ni}}. \tag{8}$$

Here, ρ_i and ρ_n are, respectively, the ion and neutral-particle mass densities, and ν_{ni} is the neutral-ion momentum transfer collision frequency.

From the four equations (1) through (4), a single fourth-order differential equation for some component of the wave field, say b_r, may be derived, which has as a solution

$$b_r = A_1 J_1(_1k_c r) + A_2 J_1(_2k_c r). \tag{9}$$

If the resistivity is assumed to be zero, the fourth-order equation becomes second order, and the second term on the right of Eq. (9) disappears. The Neumann functions have been ignored, since they lead to infinite fields at r = 0.

The allowed values of ${}_1k_c$ and ${}_2k_c$ and the ratio A_1/A_2 are determined by the boundary conditions at the radial boundary of the plasma column. Experiments[13] have shown that a realistic boundary condition that leads to accord between theory and experiment is a conducting wall with a thin insulating layer that separates the wall from the plasma. For definiteness, let the conducting wall be at $r = b$ and the plasma-insulator boundary be at $r = c < b$.

Most of the conditions encountered in the experiment are met by assuming the plasma resistivity to be zero. Under these conditions Eq. (9) becomes simply

$$b_r = A_1 J_1(k_c r) , \tag{10}$$

and it can be shown that the appropriate condition on k_c is

$$J_1(k_{cn} c) = 0 , \tag{11}$$

which defines the possible values of $k_{cn}c$ as roots of J_1. The n is now used to denote the root number. The relation between p and ω is

$$p_n^2 = \frac{k_{cn}^2}{2}\left(\frac{2\beta_n^2}{1-r^2} - \left\{1 - \left[1 + 4\beta_n^4 \frac{r^2}{(1-r^2)^2}\right]^{1/2}\right\}\right) . \tag{12}$$

[The second hydromagnetic mode is described by changing the sign of the square-root term of Eq. (12)]. Here $\beta_n = \omega/vk_{cn}$ and $r = (\omega/\omega_{ci})(\rho/nm_i)$.

In the vicinity of the resonance where $\omega = \omega_{ci}$, the resistive term becomes relatively important and cannot be ignored. To treat this case, it is necessary to assume that the insulating layer at the tube wall is thin. Specifically, we require

$$a = \frac{v^2}{c^2}\,\frac{k_{cn}}{p^2} \ll (b-c) \ll \frac{1}{k_{cn}} , \tag{13}$$

where $a = \eta\omega/\mu_0 v^2$, $v = B/(\mu_0\rho)^{1/2}$, and c = velocity of light. The lower limit corresponds to a condition that the capacitive reactance of the insulating layer be large compared with the resistance of an equal thickness of plasma.

In this case b_r is given approximately by Eq. (10), and the condition on k_{cn} is given by Eq. (11). The dispersion relation between p and ω is

$$p_n^2 = \frac{k_{cn}^2}{2(1-ia)^2-2r^2}\left(-(1-r^2)+2\beta^2(1-ia)+2a^2+3ia\right.$$

$$\left.+\left\{(1-r^2)^2+4r^2\beta^4-a^2+ia\left[2(r^2-1)+4r^2\beta^2\right]\right\}^{1/2}\right), \qquad (14)$$

which reduces to Eq. (12) for $a = 0$. It is assumed that this equation holds over the whole range of r.

Eq. (11) has an infinite number of solutions, so we write the magnetic field as a sum

$$b_r = \sum_{n=1}^{\infty} A_n J_1(k_{cn} r). \qquad (15)$$

The other wave magnetic fields are obtained from Eqs. (1) through (4) and are

$$b_\theta = \sum_n \frac{i}{r p_n^2}\left[\frac{\omega^2}{v^2}-(1-ia)(p_n^2+k_{cn}^2)\right] A_n J_1(k_{cn} r) \qquad (16)$$

and

$$b_z = \sum_n \frac{i}{p_n} k_{cn} A_n J_0(k_{cn} r). \qquad (17)$$

The real and imaginary parts of p are the propagation constant k and the attenuation constant α, respectively. Plots of k and α as functions of axial magnetic field from Eq. (14) are presented in Fig. 1 for various plasma densities.

The coefficients of A_n of Eq. (15) are determined by the driving-electrode geometry. In this experiment, the waves are induced by a current flow between coaxial electrodes, the inner one of radius a and the outer one of radius b. Within the end insulator, the magnetic field must be symmetric and azimuthal, and have a 1/r dependence. This field is matched across the insulator-plasma

boundary to the b_θ plasma field. On the electrode surfaces the tangential electric fields must be zero; this requirement leads to a condition that b_θ also be zero at the electrode surface. Thus b_θ is

$$b_\theta(r) = \frac{\mu_0 i}{2\pi r}, \quad \text{for } a < r < b, \tag{18}$$

$$= 0, \quad \text{for } r < a, \ r > b.$$

This function is now expanded in a series of Bessel functions, and the coefficients are matched to the A_n of Eq. (15). We find

$$A_n = \frac{2ip^2 r}{p^2 + k_{cn}^2} \left\{ -\frac{\mu_0 i}{2\pi k_{cn}} \frac{[J_0(k_{cn}c) - J_0(k_{cn}a)]}{c^2 J_0^2(k_{cn}c)} \right\} . \tag{19}$$

Higher modes are distinguished by larger values of k_{cn}, and Eq. (14) shows that these are subject to progressively higher damping. Figure 2 shows plots of k and ϵ against B for the lowest few modes, demonstrating the higher attenuation of higher modes. However, for propagation lengths less than 0.5 m the fifth mode is seen to suffer negligible damping for magnetic fields removed by 1 kilogauss or more from resonance.

In order for the above results to be applicable to the case of a spatially varying axial magnetic field, it is sufficient that $\partial B/\partial z \ll kB$ or that the axial field change slowly over a wavelength of the wave field. If this condition holds, then k and ϵ should be given locally by Eq. (14) with the appropriate values of B substituted, and the phase of the wave field should be given by

$$\phi = \int_0^z k(z)\, dz . \tag{20}$$

If the axial field should change appreciably in a distance comparable to the hydromagnetic wavelength, then reflections are expected to occur.

Again, if the attenuation is negligible, the energy flux through any cross section of the plasma must be constant. Since the wave velocity decreases with B, the wave amplitude must increase correspondingly to conserve energy. A result of this requirement is that the coefficients A_n and c_n should vary directly with $k^{1/2}$. Thus, we expect the amplitude of b_θ to increase as the wave propagates into the decreasing magnetic field until, near the resonance region, the rate of attenuation rapidly increases, and the amplitude of b_θ drops as the wave energy is lost.

EXPERIMENTAL ARRANGEMENTS

The plasma is produced from deuterium gas at 5.0×10^{-3} torr pressure and is contained in a copper cylinder 19.8 cm in diameter and 94.0 cm long, as shown in Fig. 3. The magnetic field is supplied by the coils shown and is normally set to provide a mirror field of approximately 10 kG at the midplane and 20 kG at the ends. These fields correspond approximately to the ion cyclotron fields of $B_i = \omega M/e$ and $2B_i$, respectively, where ω is the angular wave frequency and M and e are the mass and charge, respectively, of the deuterium ion. The copper cylinder is closed by quartz end plates in one of which is mounted a centered 6.25-cm diameter 7.5-cm long molybdenum electrode. Mounted inside the copper cylinder, coaxial with the center electrode, is an outer electrode the inner radius of which is made to intersect those magnetic field lines that just miss the cylinder walls at the center of the magnetic mirror.

These coaxial electrodes are connected via the lines and ignitron switch shown to a capacitor that supplies a radial electric field to the plasma. The radial field produces an ionizing front of the type previously studied.[14] The front proceeds down the cylinder, leaving a highly ionized rotating plasma behind it. When the front arrives at the opposite end of the cylinder, the gross

rotation of the plasma is stopped by short-circuiting the electrodes with the other ignitron shown in Fig. 3. To reduce the turbulence generated either by this braking action or by the later application of the wave-driving fields, a copper screen is mounted at the end of the cylinder opposite the electrodes.[15] Although initial ion-density measurements of the specific plasma prepared in this manner have not been made, it is expected to be close to the initial neutral density--in keeping with the results obtained at higher densities with similar geometries, fields, and energy transfer.[13]

Approximately 30 μsec after the electrodes have been short-circuited, an 8.3-Mc electric field is applied for 1.0 msec; the radio frequencies are isolated from the circuitry supplying the ionizing front. Figure 4 shows oscilloscope traces of the 8.3-Mc current and voltage supplied to the electrodes. The 8.3-Mc oscillator is capable of 1.2-MW power output, although it was not operated at full output in the experiments described here. At the oscillator power level used, wave measurements made later than 250 μsec after the oscillator is turned on are insensitive to moderate variation in the ionizing conditions such as the level and time duration of the voltage driving the initial ionizing front.

WAVE-FIELD MEASUREMENTS

The wave magnetic fields were measured by using five 0.42-cm-diameter four-turn coils spaced at 1.27-cm intervals inside a 0.8-cm-diameter glass tube. This tube was positioned along a radius of the discharge cylinder in such a manner that the radial dependence of b_θ could be obtained at any axial position in the cylinder. Figure 5 shows $b_\theta(r)$ at four axial positions 800 μsec after the wave-inducing field is applied. The general behavior is as expected; the solid curves drawn through the experimental data at +25 cm and at +10 cm are

proportional to 1/r. The 1/r dependence is preserved over most of the path, in keeping with the results of the calculations shown in Fig. 2. The wave fields increase as the wave propagates toward lower magnetic fields, then decrease to low values as the ion cyclotron resonance is encountered. Variations in the wave-field amplitudes amounting to approximately ± 15% of those amplitudes shown in Fig. 5 were observed from one discharge to another. Not shown in Fig. 5 are the wave fields in regions connected to the electrodes along common magnetic-field lines. In these regions, which are designated by the vertical bars, the wave fields are both small and nonreproducible.

Figure 6 shows in a more detailed manner than Fig. 5 the amplitude of b_θ as a function of axial position. These measurements were made at a constant radius midway between the electrodes. A sharp decrease in amplitude near resonance is apparent, as is the slow increase in amplitude over most of the path due to the decrease of wave velocity. Amplitude variations of approximately ± 15% of the values shown also occurred in these measurements.

The amplitude of the radial component of the wave field b_r has also been studied. Two features of the behavior of this component have emerged. First, the time dependence of the amplitude is much more marked than with b_θ. Second, except in the resonance region the ratio of amplitudes b_r/b_θ is uniformly larger than is expected on the basis of the calculations outlined above. Both effects suggest that some mechanism other than pure wave propagation along a decreasing magnetic field is responsible for transferring some magnetic-field energy from the b_θ to the b_r component. On the other hand, in the resonance region the ratio b_r/b_θ is very nearly unity at all times--as is expected for resonant ion motions.

The wave velocity can be determined from the z dependence of the wave phase. With the approximations discussed above, where the waves are propagated in a region of spatially varying magnetic field, the phase shift is given by $\phi(z) = \int_0^z k(z)\, dz$.

Figure 7 gives the b_θ phase shift with z at 800 μsec after application of the wave field. The points shown were obtained from a succession of shots taken at the various axial positions with the probe described above. The relatively large scatter is due to shot-to-shot variations between the wave-field phases and those of the radio-frequency drive current with which they are compared.

The wave velocity and hence plasma density may be obtained by fitting Eqs. (14) and (20) to the experimental phase data of Fig. 7. The solid curve in Fig. 7 is a plot of $\phi(z)$ for an ion density of 0.2×10^{-7} kg/m^3. The fit near the driving end is quite close. As resonance is approached, the phase measurements become increasingly unreliable, and the data depart from the solid curve. A comparison of the ion density given by the above fit and the initial neutral deuterium density of 11.8×10^{-7} kg/m^3 indicates that approximately 1.7% of the initial density remains after 800 μsec.

A further measure of the ion density may be obtained from the impedance of the device considered as a plasma-filled wave guide. The impedance of such a guide is given by

$$z = z_0/K^{1/2},$$

where z_0 is the vacuum impedance of the guide and K is the dielectric constant given by

$$K = 1 + (\mu_0 \rho c^2/B^2).$$

The measured impedance of the plasma (i.e., the ratio of the driving voltage to the driving current) at 800 μsec is 1.48 ohm; the ion density corresponding to this impedance is 0.26×10^{-7} kg/m^3. From Fig. 4 it is clear that the impedance increases monotonically--indicating a continual decrease in density during application of the wave fields. Densities calculated on the basis of Fig. 4 decrease by a factor of 5.4 from 100 μsec to 800 μsec.

The densities described above have not been confirmed by other techniques. However, the indication is that a considerable portion of the initial plasma is removed from the wave-propagation region by action of the wave fields.

WAVE ENERGY

With the wave-field data given above it is possible to calculate the energy content of the waves and to compare the wave power with that supplied by the oscillator. The total wave energy per unit length is obtained by integration of $b_\theta^2(r)$ over the radius. By combining this energy, the observed ratio of b_r/b_θ, and the wave velocity determination made from the phase shift data, the total wave power is found to be 250 kW. The corresponding total input power from the oscillator at 800 μsec is 380 kW. Thus the efficiency of power transfer from the oscillator into hydromagnetic wave motion is roughly 65%. Beyond the mid-plane at -10 cm the wave amplitude is approximately 8 G, compared with 31 G at +10 cm; thus, an energy loss across the resonance region in the ratio of 15:1 is implied.

CONCLUSION

From these experiments it is concluded that a substantial portion of the power from the oscillator can be coupled into torsional hydromagnetic waves in a highly ionized plasma by direct application of an oscillatory radial electric field. These waves propagate in a relatively steep magnetic mirror geometry to an ion cyclotron resonance region at the mirror center, where at least 90% of the wave energy is lost from the wave.

APPENDIX

Ion Orbits

The nature of collisionless ion orbits in a hydromagnetic wave may be visualized by inspection of the solution of the equation of motion of an ion,

$$[\underline{E} + (\underline{v} \times \underline{B})]\, q = m\dot{\underline{v}} . \tag{A1}$$

In a small volume element, the wave electric field is generally elliptically polarized, approaching circular polarization as the wave approaches ion cyclotron resonance. The wave electric field is determined from the wave magnetic field by Maxwell's equation

$$\nabla \times \underline{E} = -\dot{\underline{b}} . \tag{A2}$$

The solution of the equation of motion contains two terms, showing that the motion consists of the usual cyclotron motion superimposed upon a guiding-center motion. The guiding-center motion is elliptical with its major axis perpendicular to the major axis of the elliptically polarized E field. The guiding-center ellipse enlarges and becomes circular as resonance is approached.

Some ion orbits and guiding-center ellipses are illustrated in Figs. 8 and 9 for parameters listed in Table AI. As the wave approaches resonance ($\omega_c/\omega \to 1$), the superposition of these two motions becomes an alternation of accelerating spirals and decelerating spirals. In the limit $\omega_c/\omega = 1$, the accelerating spiral grows without bound.

The first series of orbit diagrams (Fig. 8) illustrates the effect of increasing the wave frequency while other parameters are held constant. Using 1 eV as the energy associated with the cyclotron motion, the transition is shown from a low-frequency, approximately plane-polarized wave to a near-resonant circularly polarized wave.

The second series of orbit diagrams (Fig. 9) shows collisionless orbits under conditions similar to those in the present experiment. The principal variable in this series is the external magnetic field, which decreases in such a way as to simulate wave propagation down the chamber toward the resonant field. The size of the guiding center ellipse is determined by experimentally determined wave amplitudes. The cyclotron energy is taken equal to 18 eV.

Table AI. Parameters of ion-orbit diagrams

Figure No.	Freq. (Mc)	B (W/m^2)	ω_c/ω	b_r/b_θ
8	0.64	1.3	15.0	0.005
	1.95	1.3	5.0	0.015
	6.45	1.3	1.5	0.036
	8.3	1.3	1.167	0.168
9	8.3	1.7	1.525	0.036
	8.3	1.5	1.345	0.0662
	8.3	1.4	1.256	0.099
	8.3	1.2	1.078	0.367

References and Footnote

* Work done under the auspices of the U. S. Atomic Energy Commission.

1. T. K. Allen, W. R. Baker, R. V. Pyle, and J. M. Wilcox, Phys. Rev. Letters 2, 383 (1959).
2. J. M. Wilcox, F. I. Boley, and A. W. DeSilva, Phys. Fluids 3, 15 (1960).
3. A. W. DeSilva, Experimental Study of Hydromagnetic Waves in Plasma (Ph. D. Thesis) Lawrence Radiation Laboratory Report UCRL-9601, March 1961.
4. A. Nagao and T. Sato, J. Phys. Soc. Japan 15, 735 (1960).
5. A. Nagao and T. Sato, Research Report, Tohoku University, Sendai, Japan, 1961.
6. W. M. Hooke, F. H. Tenney, M. H. Brennan, H. M. Hill, and T. H. Stix, Phys. Fluids 4, 1131 (1961).
7. N. I. Nazarov, A. I. Ermakov, A. S. Lobko, V. A. Bondarev, V. T. Tolok, and K. D. Sinelnikov, Paper CN-10/231, IAEA Conference on Plasma Physics and Controlled Nuclear Fusion Research, Salzburg, 1961.
8. T. H. Stix, Phys. Fluids 1, 308 (1958).
9. R. Gajewski, Phys. Fluids 2, 633 (1959).
10. W. A. Newcomb, in Magnetohydrodynamics, edited by R. K. Landshoff (Stanford University Press, Stanford, California, 1957), p. 109.
11. A. Banos, Proc. Roy. Soc. (London) A233, 350 (1955).
12. L. Spitzer, Jr., The Physics of Fully Ionized Gases (Interscience Publishers, Inc., New York, 1956), p. 35.
13. J. M. Wilcox, A. W. DeSilva, and W. S. Cooper III, Phys. Fluids 4, 1506 (1961).

14. J. M. Wilcox, W. R. Baker, F. I. Boley, W. S. Cooper III, A. W. DeSilva, and George R. Spillman, Devices for Generating Highly Ionized Hydrogen Plasma (UCRL-10121, May 7, 1962), J. Nucl. Energy, Pt C (to be published).

15. J. M. Wilcox, W. S. Cooper III, A. W. DeSilva, G. R. Spillman, and F. I. Boley, J. Appl. Phys. 33, 2714 (1962).

Figure Captions

Fig. 1. Propagation constant k and attenuation constant ϵ plotted as a function of the magnetic field for plasma densities $\rho_1 = 0.2 \times 10^{-6}$ kg/m^3, $\rho_2 = 0.2 \times 10^{-7}$ kg/m^3, and $\rho_3 = 0.2 \times 10^{-8}$ kg/m^3.

Fig. 2. Propagation constant k and attenuation constant ϵ plotted as a function of magnetic field for propagation modes 1, 3, and 5.

Fig. 3. Experimental apparatus.

Fig. 4. Oscilloscope traces of 8.3 Mc voltage (upper trace 2300 V/cm) and current (lower trace 900 A/cm) supplied to coaxial electrodes. Total sweep time is 1.0 msec.

Fig. 5. Wave field $b_\theta(r)$ at four axial positions 800 μsec after rf start. Amplitude variations of ± 15% of those shown were observed.

Fig. 6. Wave field $b_\theta(z)$ at a constant radius as a function of axial position 800 μsec after rf start. Amplitude variations of ± 15% of those shown were observed.

Fig. 7. Phase shift of b_θ wave field as a function of axial position 800 μsec after rf start.

Fig. 8. Ion orbits for various wave frequencies (with wave amplitude and wave number held constant), as an illustration. The orbits increase from 1 mm in major diameter to 3 mm as resonant conditions are approached. Dashed lines represent guiding-center motion, and solid lines the particle motion.

Fig. 9. Ion orbits (under conditions similar to those of this experiment) that simulate a wave propagating along a decreasing magnetic field toward the resonant field. These orbits are of the order of 3 mm in major diameter.

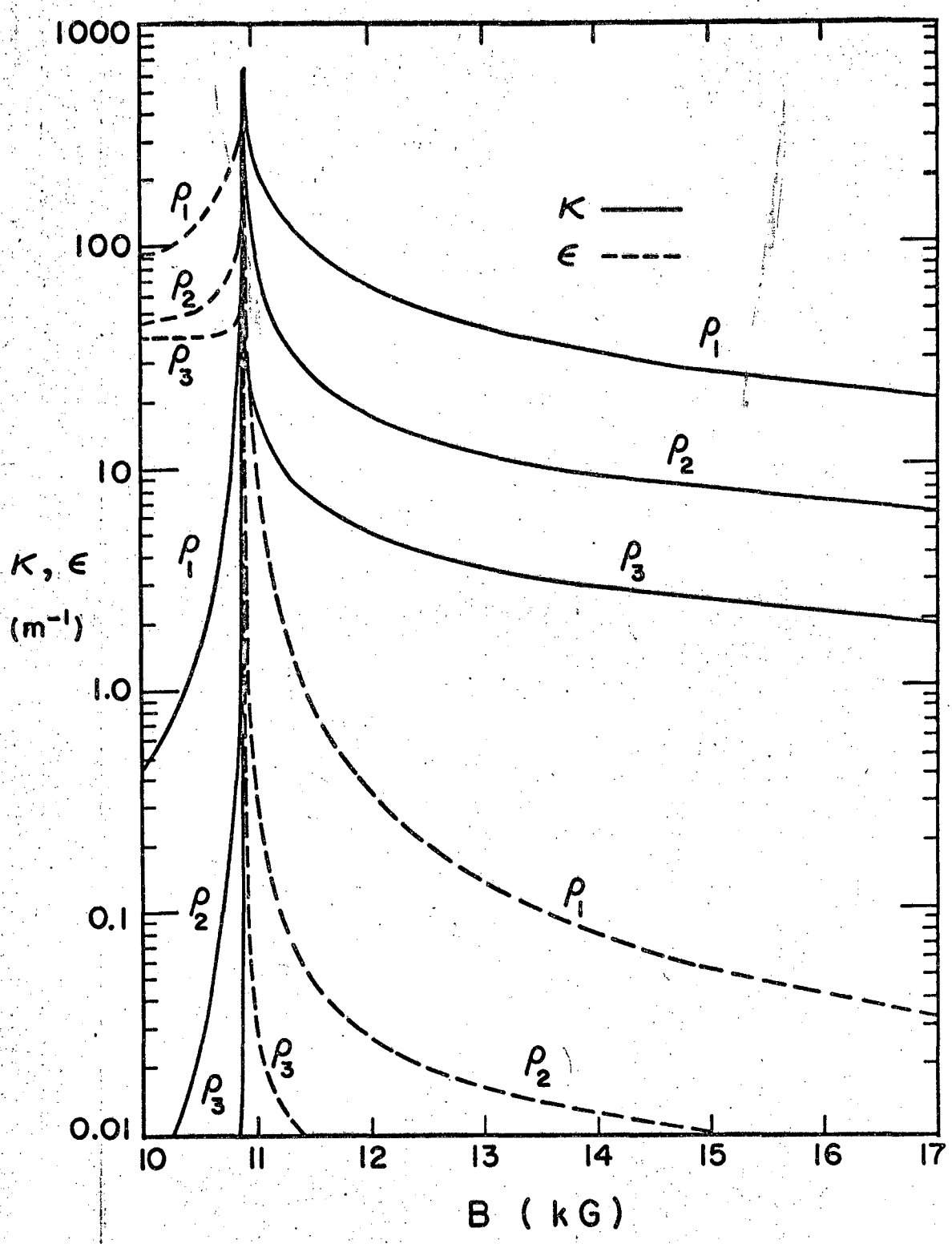

MU-27645

Fig. 1

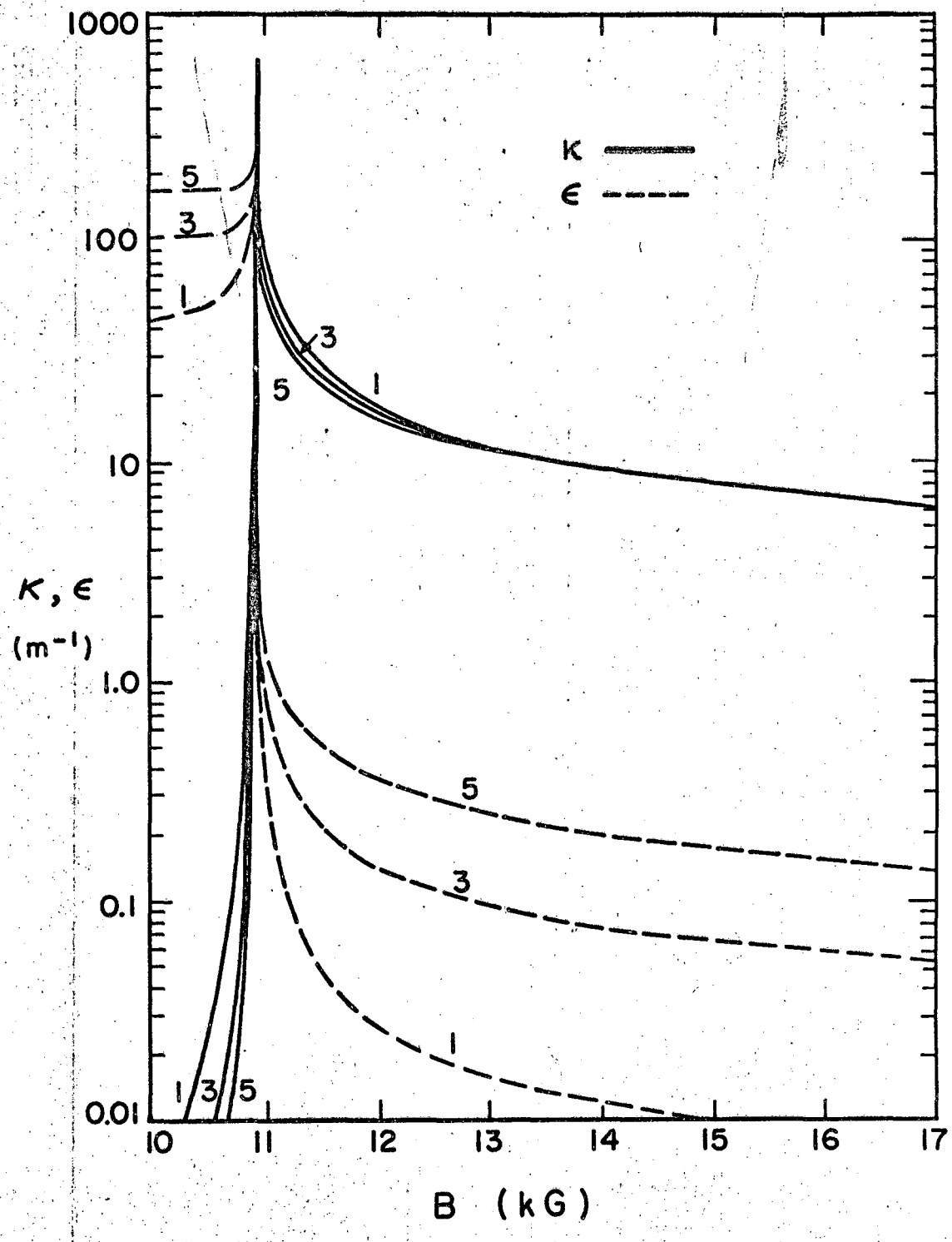

MU-27646

Fig. 2

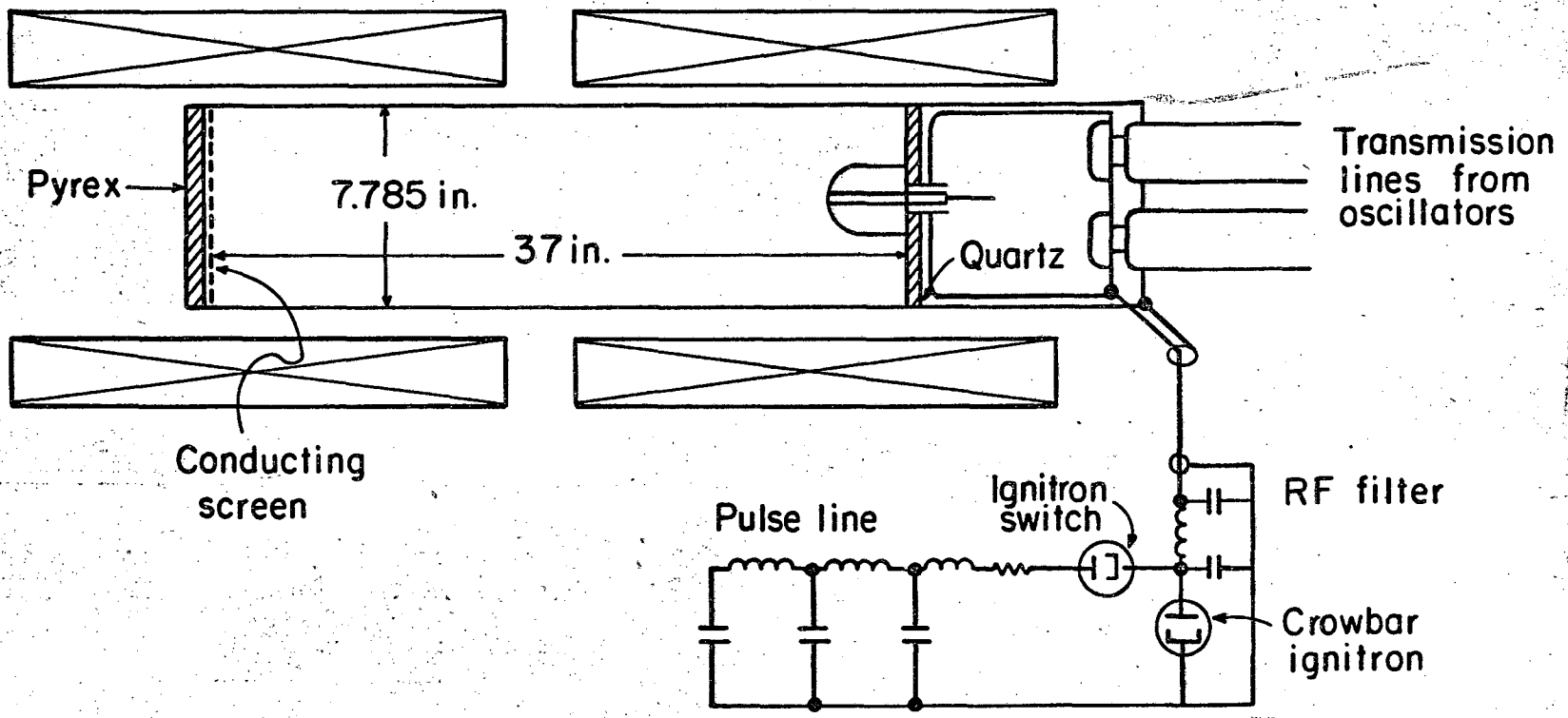
Pyrex
7.785 in.
37 in.
Quartz
Transmission lines from oscillators
Conducting screen
Pulse line
Ignitron switch
RF filter
Crowbar ignitron
MU-26410

Fig. 3

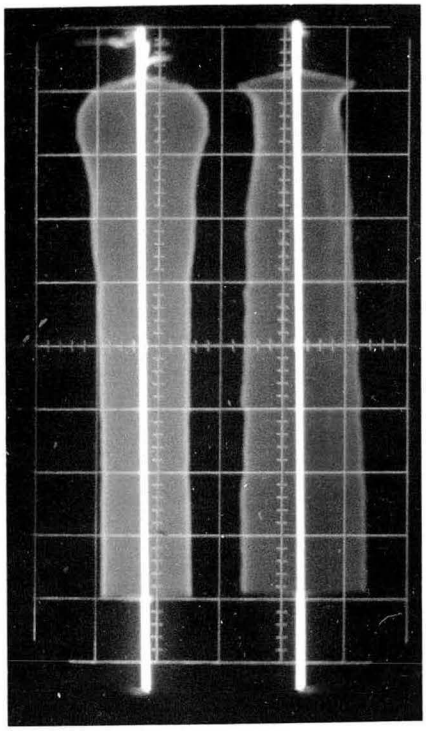

Fig. 4

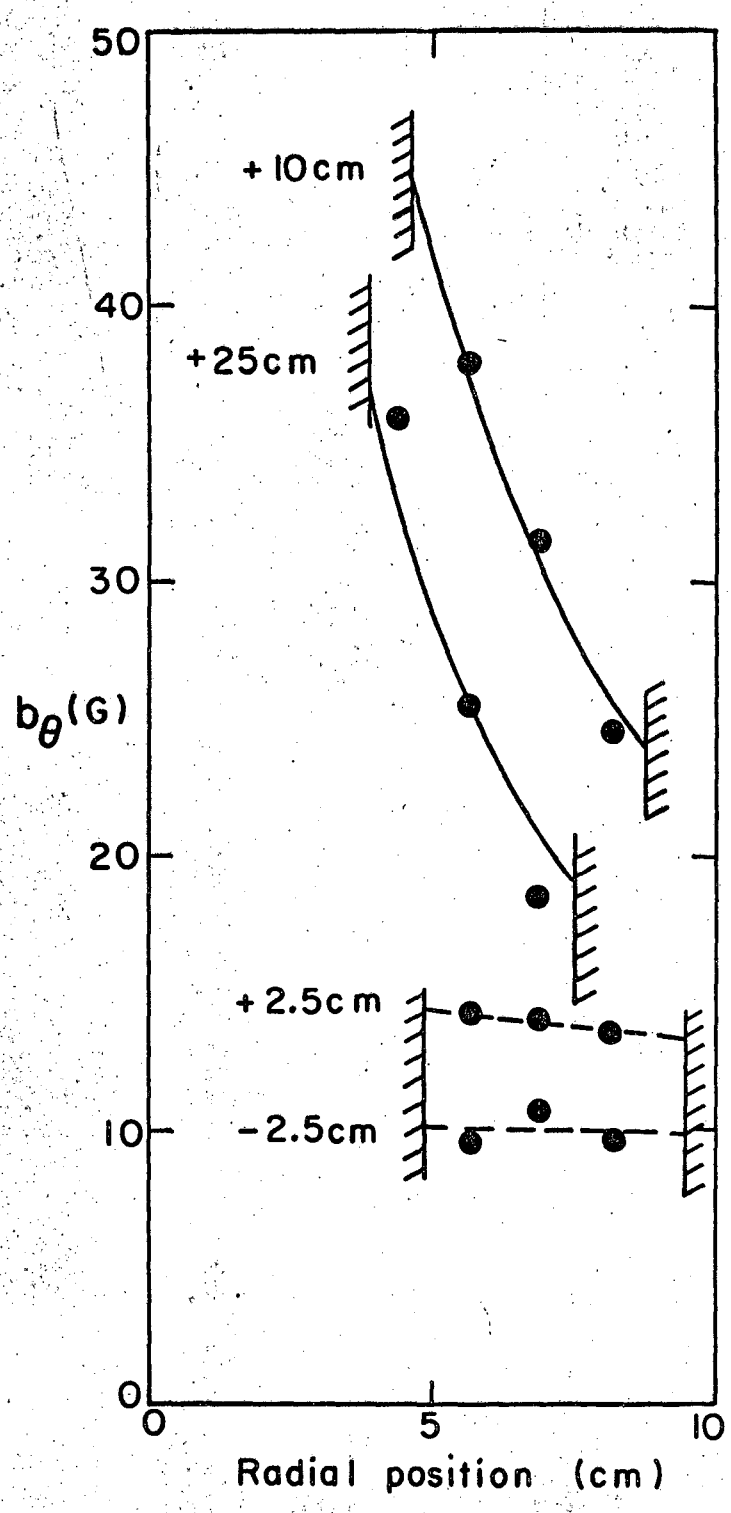
50
40
30
20
10
0
+10cm
+25cm
+2.5cm
-2.5cm
b_θ(G)
0
5
10
Radial position (cm)
MU-27647

Fig. 5

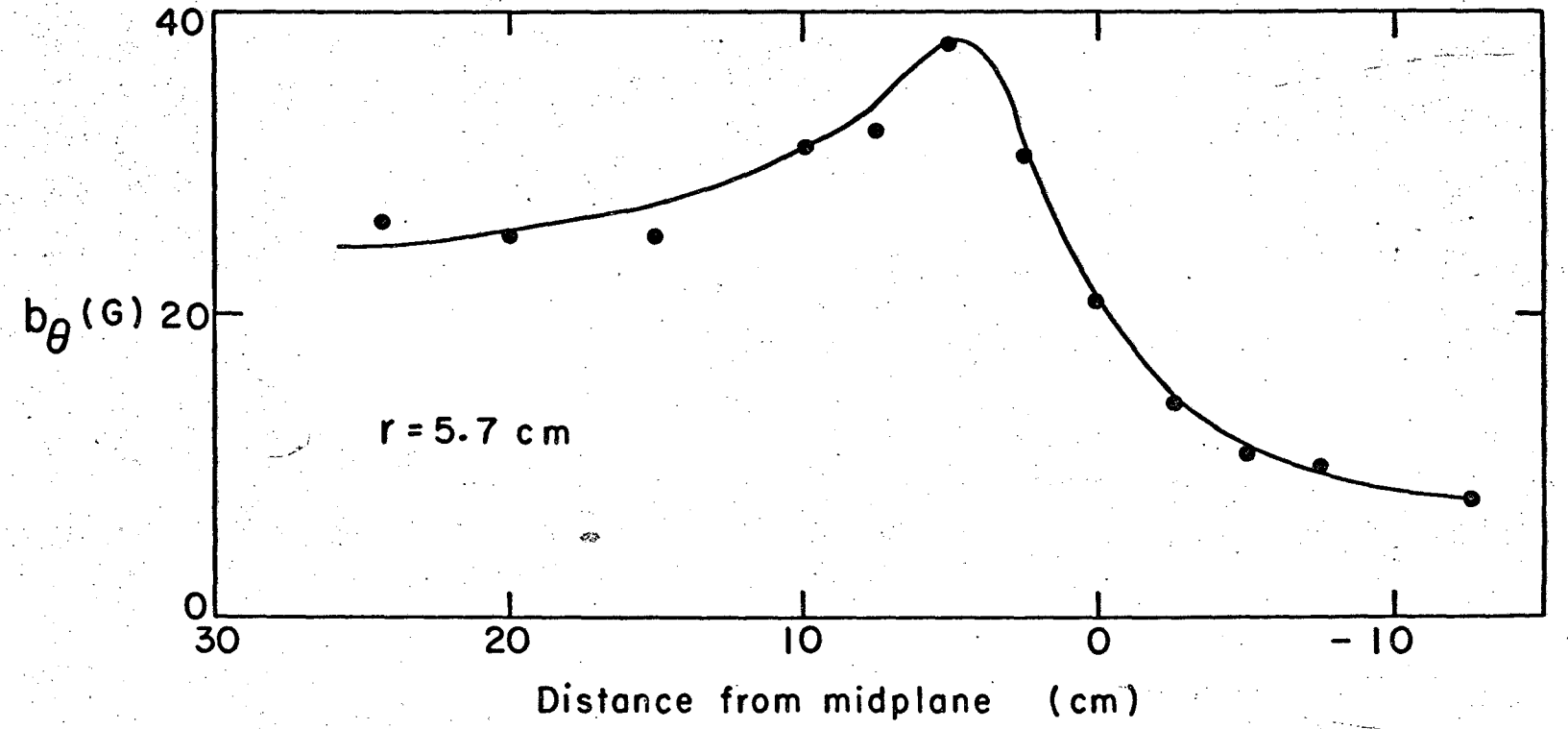

MU-27648

Fig. 6

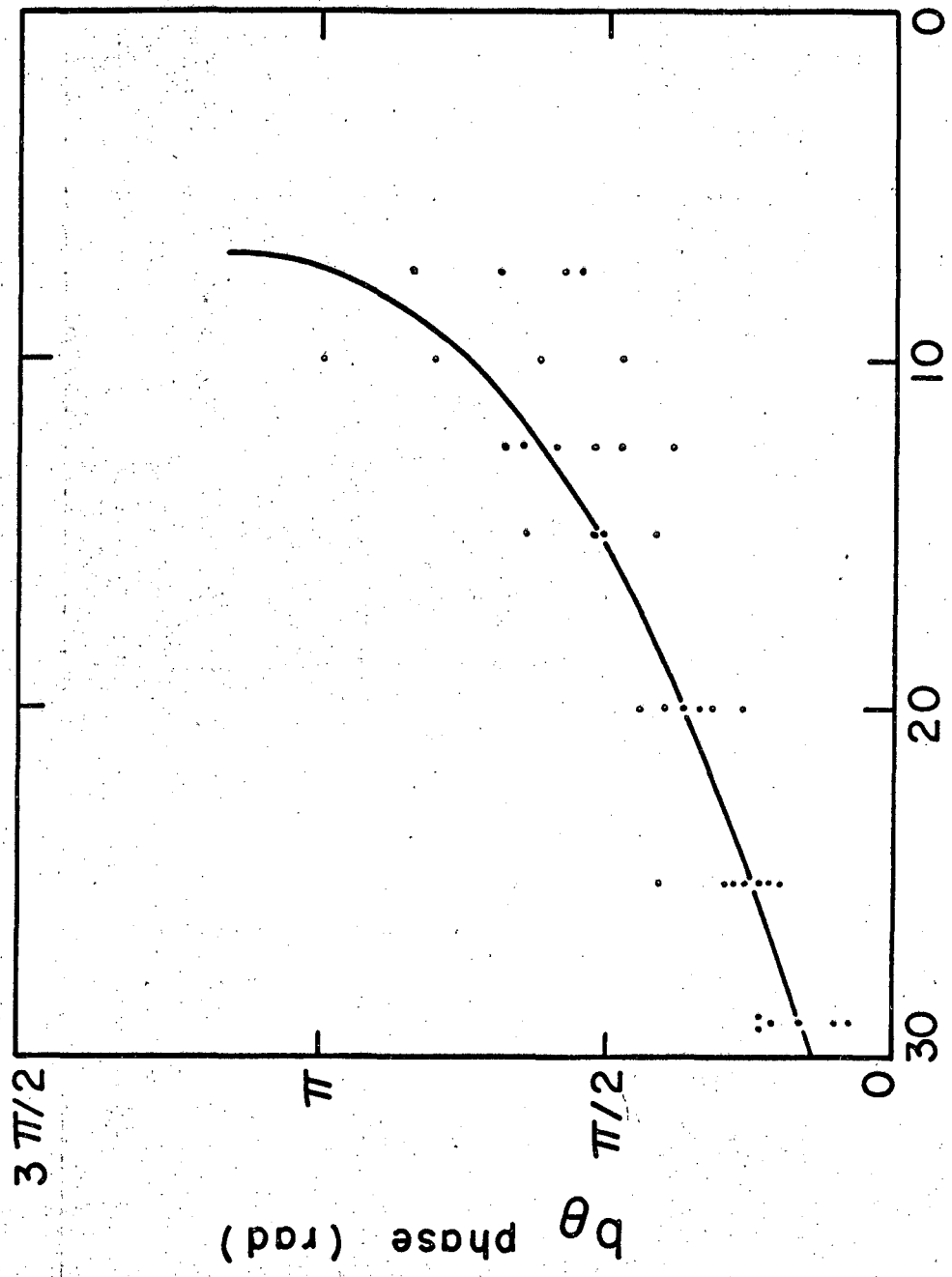
3π/2
π
π/2
0
b_θ phase (rad)
0
10
20
30
Distance from midplane (cm)
MU-27649

Fig. 7

$\omega_c / \omega = 15.0$

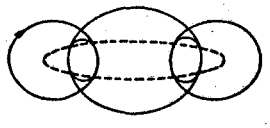

$\omega_c / \omega = 5.0$

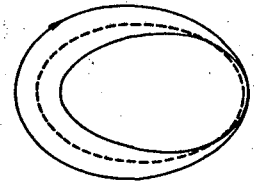

$\omega_c / \omega = 1.5$

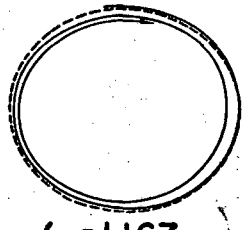

$\omega_c / \omega = 1.167$

MUB-1398

Fig. 8

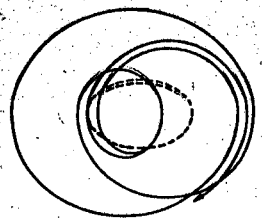

$\omega_c/\omega = 1.52$

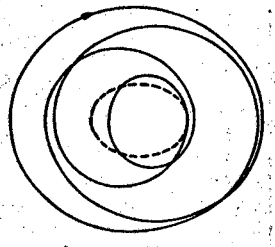

$\omega_c/\omega = 1.345$

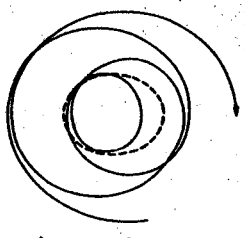

$\omega_c/\omega = 1.256$

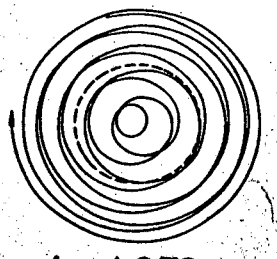

$\omega_c/\omega = 1.078$

MUB-1397

Fig. 9

This report was prepared as an account of Government sponsored work. Neither the United States, nor the Commission, nor any person acting on behalf of the Commission:

A. Makes any warranty or representation, expressed or implied, with respect to the accuracy, completeness, or usefulness of the information contained in this report, or that the use of any information, apparatus, method, or process disclosed in this report may not infringe privately owned rights; or

B. Assumes any liabilities with respect to the use of, or for damages resulting from the use of any information, apparatus, method, or process disclosed in this report.

As used in the above, "person acting on behalf of the Commission" includes any employee or contractor of the Commission, or employee of such contractor, to the extent that such employee or contractor of the Commission, or employee of such contractor prepares, disseminates, or provides access to, any information pursuant to his employment or contract with the Commission, or his employment with such contractor.